



IMPLEMENTING MULTI-SCALE AGRICULTURAL INDICATORS EXPLOITING SENTINELS

**VEGETATION FIELD DATA AND PRODUCTION OF
GROUND-BASED MAPS:**

**“25 DE MAYO SITE, LA PAMPA, ARGENTINA”
7TH - 9TH FEBRUARY 2014**

ISSUE I1.00

EC Proposal Reference N° FP7-311766

Actual submission date : May 2014

Start date of project: 01.11.2012

Duration : 40 months

Name of lead partner for this deliverable: EOLAB

Book Captain: Consuelo Latorre (EOLAB)

Contributing Authors: Fernando Camacho, Margarita Pérez (EOLAB)

M Eugenia Beget, Carlos Di Bella (INTA)

Project co-funded by the European Commission within the Seventh Framework Program (2007-2013)		
Dissemination Level		
PU	Public	X
PP	Restricted to other programme participants (including the Commission Services)	
RE	Restricted to a group specified by the consortium (including the Commission Services)	
CO	Confidential, only for members of the consortium (including the Commission Services)	

DOCUMENT RELEASE SHEET

Book Captain:	C. Latorre	Date: 26.05.2014	Sign. 
Approval:	R. Lacaze	Date: 24.06.2014	Sign. 
Endorsement:		Date:	Sign.
Distribution:			

CHANGE RECORD

Issue/Revision	Date	Page(s)	Description of Change	Release
	26.05.2014	All	First Issue	I1.00

TABLE OF CONTENTS

1. Background of the Document.....	10
1.1. Executive Summary	10
1.2. Portfolio	10
1.3. Scope and Objectives.....	11
1.4. Content of the Document	11
2. Introduction	12
3. Study area.....	14
3.1. Location	14
3.2. Description of The Test Site	15
4. Ground measurements.....	18
4.1. Material and Methods	18
4.1.1. System Calibration.....	18
4.1.2. CAN-EYE Software description	20
4.2. Spatial Sampling Scheme	22
4.3. ground data.....	24
4.3.1. Data processing	24
4.3.2. Content of the Ground Dataset.....	27
5. Evaluation of the sampling	30
5.1. Principles.....	30
5.2. Evaluation Based On NDVI Values.....	30
5.3. Evaluation Based On Convex Hull: Product Quality Flag.	31
6. production of ground-based maps	33
6.1. Imagery	33
6.2. The Transfer Function.....	33
6.2.1. The regression method.....	33
6.2.2. Band combination	34
6.2.3. The selected Transfer Function	34
6.3. The High Resolution Ground Based Maps	37
6.3.1. Selected zones for validation.....	39
7. Conclusions	41



8. Acknowledgements..... 42

9. References 43

LIST OF FIGURES

Figure 1: People involved in the Field Campaign.....	13
Figure 2: Location of 25 de Mayo site in La Pampa, Argentina.....	14
Figure 3: False color composition of TOA Reflectance SPOT5 image over the study area (9 th , February 2014). ..	15
Figure 4: Examples of the different land cover types in 25 de Mayo site - La Pampa, Argentina.	16
Figure 5: Typical shrub species in 25 de Mayo site, La Pampa – Argentina	17
Figure 6: Alignment of the system formed by the camera + sigma lens.	18
Figure 7: Results of the calibration of CANON EOS 6D carried out by CAN-EYE software.....	19
Figure 8: Image with different COIs for the CANON 6D and the sigma lens. Red circle at 60° is the limit of the useful area selected for processing.	20
Figure 9: Distribution of the sampling units (ESU) over the study area. DHP sampling (in orange), PASTIS sampling (in green) over 25 de Mayo site, Argentina.	23
Figure 10: Digital Hemispherical Photographs acquired in 25 de Mayo, La Pampa, Argentina during the intensive campaign of 7-9 February 2014.....	24
Figure 11: Results of the CAN-EYE processing carried out on shrubland area. (a) DHP images. (b, c) Classified images. (d) Average gap fraction and (e) the clumping factor versus view zenith angle.	25
Figure 12: DHP images for ESU 27, showing landscape (left), understory (middle), and overstory (right), 25 de Mayo Field Campaign in La Pampa – Argentina.	26
Figure 13: Several DHP images from ESU 1 (Alfalfa), 25 de Mayo Field Campaign in La Pampa – Argentina.	26
Figure 14: LA _{eff} measurements acquired in 25 de Mayo site during the campaign of February 2014. Distribution by ESUs. (AL: Alfalfa, SH: Shrubland, G: Grassland, TP: Tree Plantation, BS: BareSoil).....	28
Figure 15: LAI measurements acquired in 25 de Mayo site during the campaign of 2014.	28
Figure 16: FAPAR measurements acquired in 25 de Mayo site during the campaign of 2014.....	28
Figure 17: FCOVER measurements acquired in 25 de Mayo site during the campaign of 2014. . Distribution by ESUs. (AL: Alfalfa, SH: Shrubland, G: Grassland, TP: Tree Plantation, BS: BareSoil)	29
Figure 18: Distribution of the measured biophysical variables over the ESUs. 25 de Mayo site during the campaign of 9 th February, 2014.	29
Figure 19: Comparison of NDVI (TOA) distribution between ESUs (green dots) and over the whole image (Blue line), 25 de Mayo – La Pampa site. Argentina (9 th February 2014).....	31
Figure 20: Convex Hull test over 20x20km ² area centered at the test site: clear and dark blue correspond to the pixels belonging to the ‘strict’ and ‘large’ convex hulls. Red corresponds to the pixels for which the transfer function is extrapolating, 25 de Mayo- La Pampa (9 th February 2014).....	32
Figure 21: Test of multiple regression (TF) applied on different band combinations. Band combinations are given in abscissa (2=G, 3=RED, 4=NIR and 5=SWIR). The weighted root mean square error (RMSE) is presented in red along with the cross-validation RMSE in green. The numbers indicate the number of data used for the robust regression with a weight lower than 0.7 that could be considered as outliers.	35
Figure 22: LA _{eff} , LAI, FAPAR and FCOVER results for regression on reflectance using 4 bands combination.	36
Figure 23: Ground-based LAI maps (20x20 km ²) retrieved on the 25 de Mayo- La Pampa site (Argentina). Top: LA _{eff} . Bottom: LAI. (9 th February 2014).....	37
Figure 24: Ground based FAPAR and FCOVER maps (20x20 km ²) retrieved on the 25 de Mayo - La Pampa site (Argentina). Top: FAPAR. Bottom: FCOVER. (9 th February 2014).	38
Figure 25: Selected areas for validation at the 3x3 km ² (in red) and 1x1 km ² (in yellow). Background HR LAI map (20x20 km ²), 25 de Mayo site, Argentina (9 th February 2014).	40

LIST OF TABLES

<i>Table 1: Coordinates and altitude of the test site (centre).....</i>	<i>14</i>
<i>Table 2: Summary of shrubland types in 25 de Mayo site.....</i>	<i>16</i>
<i>Table 3: Summary of the field measurements in 25 de Mayo – La Pampa site.</i>	<i>23</i>
<i>Table 4: The Header used to describe ESUs with the ground measurements.</i>	<i>27</i>
<i>Table 5: Acquisition geometry of SPOT5 HRG 1 N1A data used for retrieving high resolution maps.</i>	<i>33</i>
<i>Table 6: Transfer function applied to the whole site for LA_{ieff}, LAI, FAPAR and FAPAR. RW for weighted RMSE, and RC for cross-validation RMSE.</i>	<i>34</i>
<i>Table 7: Mean values and standard deviation (STD) of the HR biophysical maps for the selected 3 x 3 km² areas at 25 de Mayo site.....</i>	<i>39</i>
<i>Table 8: Mean values and standard deviation (STD) of the HR biophysical maps for the selected 1x1 km² areas at 25 de Mayo site.....</i>	<i>39</i>
<i>Table 9: Content of the dataset.....</i>	<i>40</i>

LIST OF ACRONYMS

CCD	Charge coupled devices
CEOS	Committee on Earth Observation Satellite
CEOS LPV	Land Product Validation Subgroup
DG AGRI	Directorate General for Agriculture and Rural Development
DG RELEX	Directorate General for External Relations (European Commission)
DHP	Digital Hemispheric Photographs
ECV	Essential Climate Variables
EUROSTATS	Directorate General of the European Commission
ESU	Elementary Sample Unit
FAPAR	Fraction of Absorbed Photo-synthetically Active Radiation
FAO	Food and Agriculture Organization
FCOVER	Fraction of Vegetation Cover
GCOS	Global Climate Observing System
GEO-GLAM	Global Agricultural Geo- Monitoring Initiative
GIO-GL	GMES Initial Operations - Global Land (GMES)
GCOS	Global Climate Observing System
GMES	Global Monitoring for Environment and Security
GPS	Global Positioning System
IMAGINES	Implementing Multi-scale Agricultural Indicators Exploiting Sentinels
INTA	Instituto Nacional de Tecnología Agropecuaria
JECAM	Joint Experiment for Crop Assessment and Monitoring
LAI	Leaf Area Index
LDAS	Land Data Assimilation System
LUT	Look-up-table techniques
PAI	Plant Area Index
PROBA-V	Project for On-Board Autonomy satellite, the V standing for vegetation.
RMSE	Root Mean Square Error
SPOT /VGT	Satellite Pour l'Observation de la Terre / VEGETATION
SCI	GMES Services Coordinated Interface
TOA	Top of Atmosphere Reflectance
UCL	Université Catholique de Louvain
UNFCCC	United Nations Framework Convention on Climate Change
UTM	Universal Transverse Mercator coordinate system
VALERI	Validation of Land European Remote sensing Instruments
WGCV	Working Group on Calibration and Validation (CEOS)
WGS-84	World Geodetic System

1. BACKGROUND OF THE DOCUMENT

1.1. EXECUTIVE SUMMARY

The Copernicus Land Service has been built in the framework of the FP7 geoland2 project, which has set up pre-operational infrastructures. ImagineS intends to ensure the continuity of the innovation and development activities of geoland2 to support the operations of the global land component of the GMES Initial Operation (GIO) phase. In particular, the use of the future Sentinel data in an operational context will be prepared. Moreover, IMAGINES will favor the emergence of new downstream activities dedicated to the monitoring of crop and fodder production.

The main objectives of ImagineS are to (i) improve the retrieval of basic biophysical variables, mainly LAI, FAPAR and the surface albedo, identified as Terrestrial Essential Climate Variables, by merging the information coming from different Sentinel sensors and other Copernicus contributing missions; (ii) develop qualified software able to process multi-sensor data at the global scale on a fully automatic basis; (iii) propose an original agriculture service relying upon a new method to assess the biomass, based on the assimilation of satellite products in a Land Data Assimilation System (LDAS) in order to monitor the crop/fodder biomass production together with the carbon and water fluxes; (iv) demonstrate the added value of this agriculture service for a community of users acting at global, European, national, and regional scales.

Further, ImagineS will serve the growing needs of international (e.g. FAO and NGOs), European (e.g. DG AGRI, EUROSTATS, DG RELEX), and national users (e.g. national services in agro-meteorology, ministries, group of producers, traders) on accurate and reliable information for the implementation of the EU Common Agricultural Policy, of the food security policy, for early warning systems, and trading issues. ImagineS will also contribute to the Global Agricultural Geo-Monitoring Initiative (GEO-GLAM) by its original agriculture service which can monitor crop and fodder production together with the carbon and water fluxes and can provide drought indicators, and through links with JECAM (Joint Experiment for Crop Assessment and Monitoring).

1.2. PORTFOLIO

The ImagineS portfolio contains global and regional biophysical variables derived from multi-sensor satellite data, at different spatial resolutions, together with agricultural indicators, including the above-ground biomass, the carbon and water fluxes, and drought indices resulting from the assimilation of the biophysical variables in the Land Data Assimilation System (LDAS). The ambition of the project is to provide a full coverage of the globe, at a frequency of 10 days, merging Sentinel-3 and Proba-V data.

1.3. SCOPE AND OBJECTIVES

The main objective of this document is to describe the field campaign and ground data collected at 25 de Mayo site in La Pampa-Argentina and the up-scaling of the ground data to produce ground-based high resolution maps of the following biophysical variable:

- Leaf Area Index (LAI), defined as half of the total developed area of leaves per unit ground surface area (m^2/m^2). We focused on two different LAI quantities (for green elements):
 - An effective LAI (LAI_{eff}) derived from the description of the gap fraction as a function of the view zenith angle. In addition, effective LAI measures derived at 57.5° are also provided in the ground database.
 - An actual LAI (LAI) estimate corrected from the clumping index.
- Fraction of green Vegetation Cover (FCover), defined as the proportion of soil covered by vegetation, derived from the gap fraction between 0 and 10° of view zenith angle.
- Fraction of Absorbed Photosynthetically Active Radiation (FAPAR), which is the fraction of the photosynthetically active radiation (PAR) absorbed by a vegetation canopy. PAR is the solar radiation reaching the canopy in the $0.4\text{--}0.7\ \mu m$ wavelength region. We focused on the daily integrated FAPAR computed as the black-sky FAPAR integrated over the day. In addition, two other quantities are provided: the instantaneous 'black-sky' FAPAR at 10:00h, which is the FAPAR under direct illumination conditions at a given solar position and the 'white-sky' FAPAR, which is the FAPAR under diffuse illumination conditions.

1.4. CONTENT OF THE DOCUMENT

This document is structured as follows:

- Chapter 2 provides an introduction to the field experiment.
- Chapter 3 provides the location and description of the site.
- Chapter 4 describes the ground measurements, including material and methods, sampling and data processing.
- Chapter 5 provides an evaluation of the sampling.
- Chapter 6 describes the production of high resolution ground-based maps, and the selected "mean" values for validation.
- Finally, conclusions and references are given.

2. INTRODUCTION

Validation of remote sensing products is mandatory to guaranty that the satellite products meets the user's requirements. Protocols for validation of global LAIeff products are already developed in the context of Land Product Validation (LPV) group of the Committee on Earth Observation Satellite (CEOS) for the validation of satellite-derived land products (Fernandes et al., 2014), and recently applied to Copernicus global land products based on SPOT/VGT observation (Camacho et al., 2013). This generic approach is made of 2 major components:

- The indirect validation: including inter-comparison between products as well as evaluation of their temporal and spatial consistency
- The direct validation: comparing satellite products to ground measurements of the corresponding biophysical variables. In the case of low and medium resolution sensors, the main difficulty relies on scaling local ground measurements to the extent corresponding to pixels size. However, the direct validation is limited by the small number of sites, for that reason a main objective of ImagineS is the collection of ground truth data in demonstration sites.

The content of this document is compliant with existing validation guidelines (for direct validation) as proposed by the CEOS LPV group (Morissette et al., 2006); the VALERI project (<http://w3.avignon.inra.fr/valeri/>) and ESA campaigns (Baret and Fernandes, 2012). It therefore follows the general strategy based on a bottom up approach: it starts from the scale of the individual measurements that are aggregated over an elementary sampling unit (ESU) corresponding to a support area consistent with that of the high resolution imagery used for the up-scaling of ground data. Several ESUs are sampled over the site. Radiometric values over a decametric image are also extracted over the ESUs. This will be later used to develop empirical transfer functions for up-scaling the ESU ground measurements (e.g. Martínez et al., 2009). Finally, the high resolution ground based map will be compared with the medium resolution satellite product at the spatial support of the product.

An intensive field campaign to characterize the vegetation biophysical parameters at the 25 de Mayo (La Pampa) test site was carried out by the INTA – *Instituto Nacional de Tecnología Agropecuaria*, EOLAB and UCL- *Université Catholique de Louvain*. Moreover, INTA installed the PASTIS systems to continuous monitoring PAR over different irrigated crops in the study area.

Intensive Field Campaign:

7th -9th of February 2013.

Teams involved in field collection:

INTA: C. Di Bella, M.E Beget, D.R. Fontanella, C. Aummassane, P. Sartor

EOLAB: F. Camacho, M. Pérez

UCL: M.J. Lambert

Contact:

EOLAB Fernando Camacho (fernando.camacho@eolab.es)

INTA : Carlos di Bella (dibella.carlos@inta.gob.ar)



Figure 1: People involved in the Field Campaign.

3. STUDY AREA

3.1. LOCATION

The experimental 25 de Mayo site is located in the La Pampa Region, situated in central Argentina ($37^{\circ}55'31.37''\text{S}$, $67^{\circ}48'13.86''\text{W}$) (Figure 2).

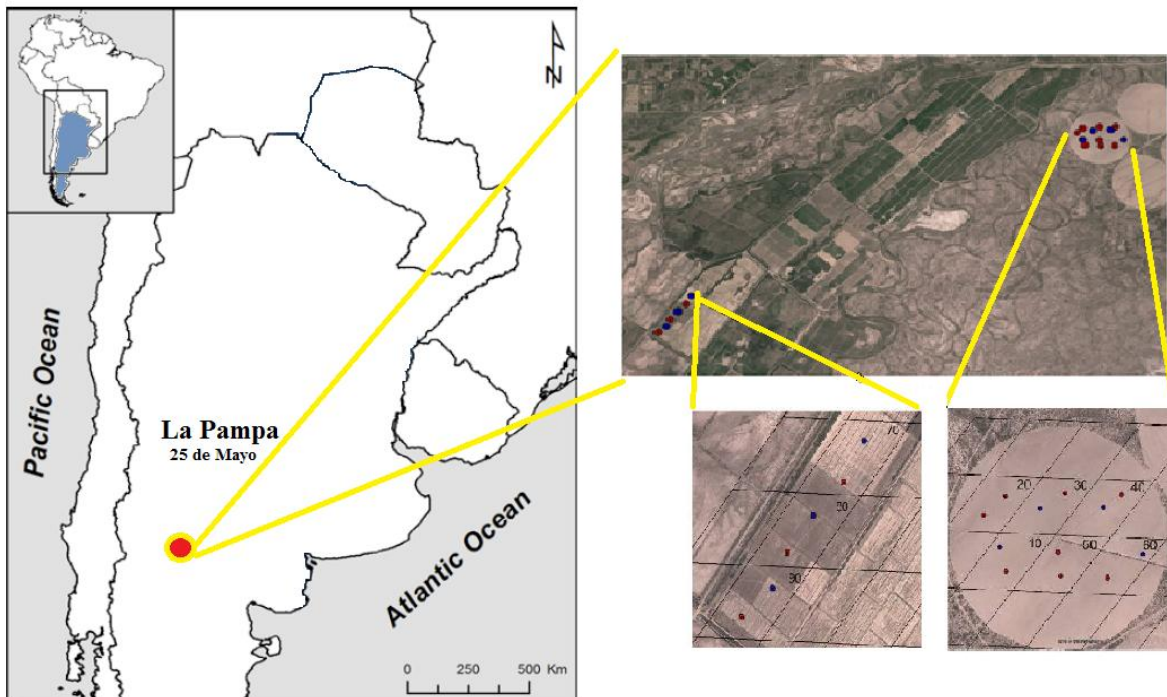


Figure 2: Location of 25 de Mayo site in La Pampa, Argentina.

Table 1: Coordinates and altitude of the test site (centre).

Site Center	
Geographic Lat/lon, WGS-84 (degrees)	Latitude = $37^{\circ}55'31.37''\text{S}$ Longitude = $67^{\circ}48'13.86''\text{W}$
Altitude	325 m

3.2. DESCRIPTION OF THE TEST SITE

The study area is located in the Section II of the Colorado River in a semi-desertic landscape dominated by shrublands, where large irrigated plots are cultivated with alfalfa and corn (Figure 3). Furthermore, other areas dedicated to tree plantation (*Populus Alba*) or grassland/fallow were identified (Figure 4). The climate in this region is semi-desertic. The average annual temperature is 14.6 °C and annual rainfall of 263 mm. The soils are sandy in texture. The dominant vegetation is shrubby type.

Shrublands of the central region of Argentina have an ecological dominant species of the genus *Larrea* (Morici et al., 2006, Cabrera, 1976). In the province of La Pampa, it covers about 35% of its surface (Table 2), followed by *Bougainvillea spinosa* (black mountain) 15.7%, *Atriplex lampa* (gobbles) 9.1% and 7.5% with *Prosopis alata*. Figure 5 shows some shrub species listed in the Table 2.

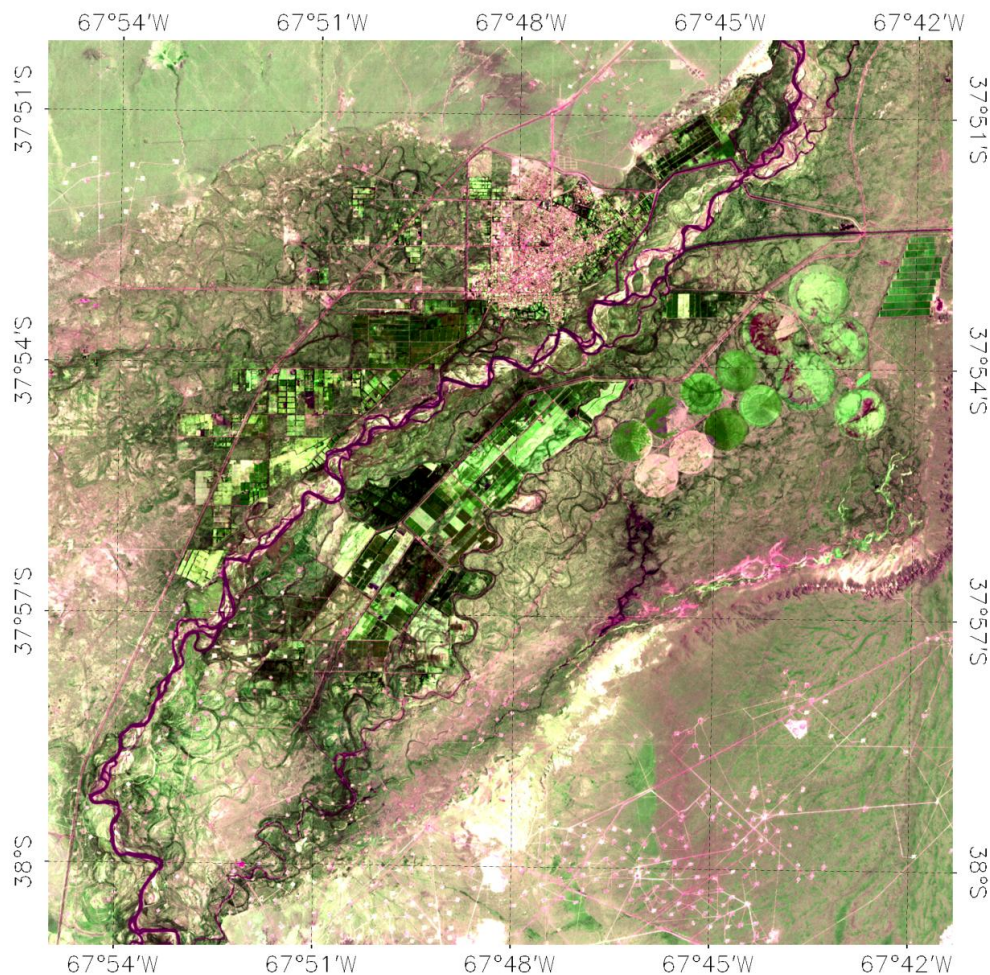


Figure 3: False color composition of TOA Reflectance SPOT5 image over the study area (9th, February 2014).

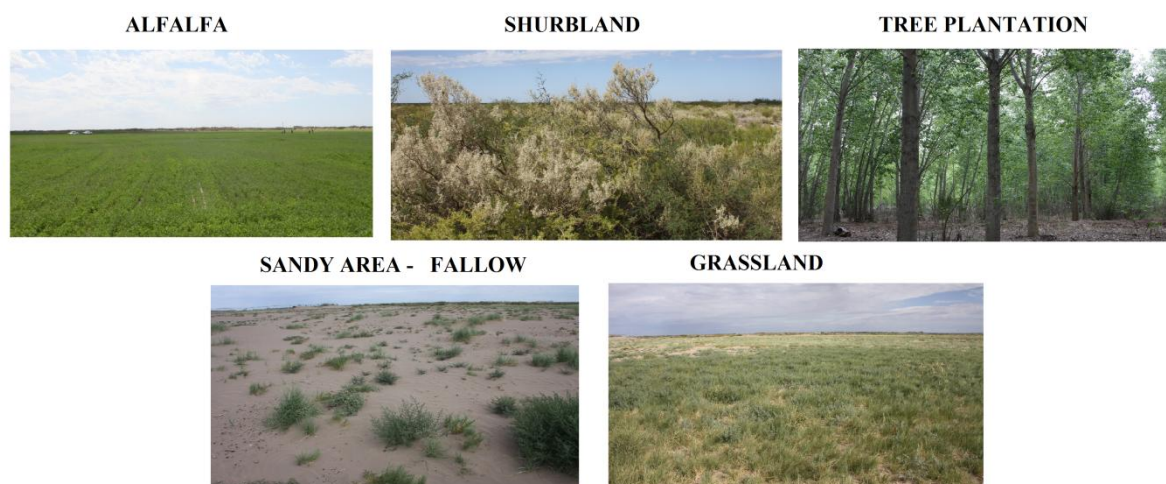


Figure 4: Examples of the different land cover types in 25 de Mayo site - La Pampa, Argentina.

Table 2 summarizes a study, carry out by the INTA, in order to characterize the dominant shrubs species in the study area. Linear transects of 50m were performed to identify the species. A total of 67 transects (3350m), separated a distance of 20m between each other, were taken. East-West direction was established.

Table 2: Summary of shrubland types in 25 de Mayo site.

SHRUB - SPECIES	NAME	NUMBER	COVER		DENSITY (plants/ha)
			m	%	
Larrea divaricata	LD	616	1151.9	34.4	906
Bougainvillea spinosa	BS	420	525	15.7	617
Atriplex lampa	AL	383	305.6	9.1	563
Prosopis alpataco	PA	155	252.2	7.5	228
Bredemeyera microphylla	BM	103	67	2	151
Acantholipia seriphiodes	AS	82	28	0.8	121
Cyclolepis genistoides	CG	71	96	2.9	104
Larrea cuneifolia	LC	66	101.9	3	97
Lycium chilense	LCHI	63	34.4	1	93
Monttea aphylla	MA	56	96.3	2.9	82
Verbena áspera	VA	44	25.4	0.8	65
Lycium gilliesianum	LG	33	15.5	0.5	49
Verbena seriphiodes	VS	4	3.3	0.1	6
chuiraga erinacea	CHE	3	4.1	0.1	4
Atamisquea emarginata	AE	3	2.5	0.1	4



Figure 5: Typical shrub species in 25 de Mayo site, La Pampa – Argentina

4. GROUND MEASUREMENTS

The ground measurement database reported here was acquired by EOLAB. It is expected to include the ground data set collected by INTA in the next version of the document.

4.1. MATERIAL AND METHODS

Several devices were used for estimating biophysical variables in the study area, including hemispherical digital photography (DHP), ceptometers and the PASTIS systems developed by INRA.

Digital Hemispheric Photographs (DHP) were acquired with a digital camera. Hemispherical photos allow the calculation of LAI, FAPAR and FCOVER measuring gap fraction through an extreme wide-angle camera lens (i.e. 180°) (Weiss et al., 2004). It produces circular images that record the size, shape, and location of gaps, either looking upward from within a canopy or looking downward from above the canopy. The system is composed by a professional camera and a fisheye lens: CANON EOS 6D and a SIGMA 8mm F3.5 – EX DG.

4.1.1. System Calibration

Optical systems are not perfect and at least two main characteristics are required to perform an accurate processing of hemispherical images.

First, the system was aligned (Figure 6), showing a few variations was found between the centre view by the objective and the centre marked in the screen of the camera. The additional calibration results were performed looking through the sight towards the target.



Figure 6: Alignment of the system formed by the camera + sigma lens.

It was needed to calibrate the system in order to determinate the Optical Centre and the Projection Function (Weiss, 2010). The optical centre is defined by the projection of the optical axis onto the CCD matrix where the image is recorded, for our dual system (camera and lens) was found in the point: (x=1378, y= 896).

Figure 7 shows the results of the system calibration generated with the CAN-EYE software developed by INRA (http://www.avignon.inra.fr/can_eye) . For both parameters (Optical Centre and Projection Function) a very good fit was achieved. The projection function is assumed to be a polar projection (angular distances (in degrees) in the object region are proportional to radial distances in pixel on the image plane). This characteristic must be also known for each focal length used (depend on selected zoom).

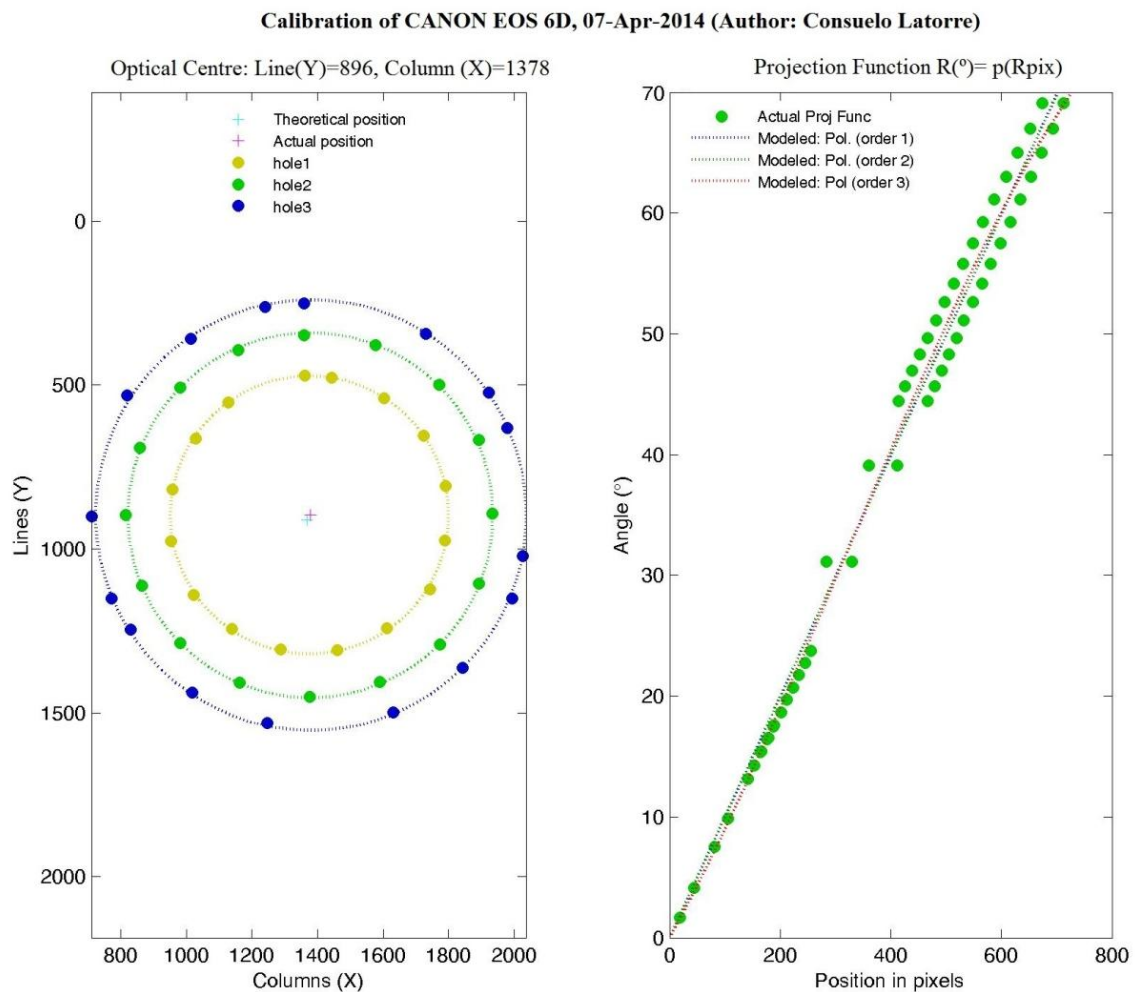


Figure 7: Results of the calibration of CANON EOS 6D carried out by CAN-EYE software.

Another important parameter is the COI (Optical Region of Interest parameter) that describes the limit of the image in viewing degrees used during the processing. It was selected the range 0° to 60° (zenith angles $> 60^{\circ}$ are not taken into account due to large occurrence of mixed pixels in these areas). Figure 8 shows different COIs over a DHP image taken with the system.

CE6D_PF201404_D1.JPG(Image Size: Y=1824, X=2736)

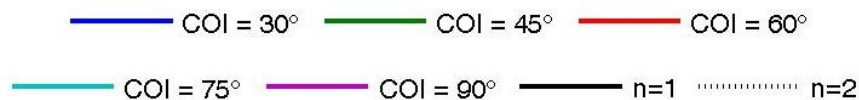
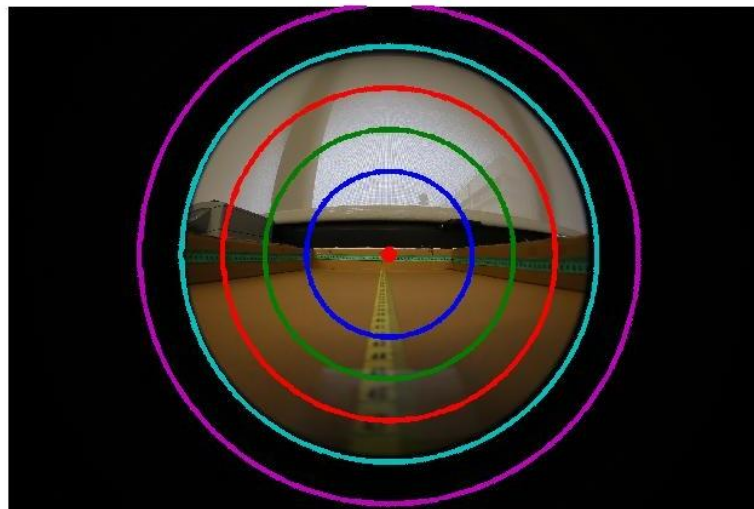


Figure 8: Image with different COIs for the CANON 6D and the sigma lens. Red circle at 60° is the limit of the useful area selected for processing.

4.1.2. CAN-EYE Software description

The hemispherical photos acquired during the field campaign were processed with the CAN-EYE software to derive LAI, FAPAR and FCOVER. It is based on a RGB colour classification of the image to discriminate vegetation elements from background (i.e., gaps). This approach allows exploiting downward-looking photographs for short canopies (background = soil) as well as upward-looking photographs for tall canopies (background = sky). CAN-EYE software processes simultaneously up to of 12 images acquired over the same ESU. Note that the 12 images were acquired with similar illumination conditions to limit the variation of colour dynamics between images.

The processing is achieved in 3 main steps (Weiss et al., 2004). First, image pre-processing is performed, which includes removing undesired objects (e.g. operator, sun glint) and image contrast adjustments to ensure a better visual discrimination between vegetation elements and background. Second, an automatic classification (k-means clustering) is applied to reduce the total number of distinctive colours of the image to 324 which is sufficient to ensure accurate discrimination capacities while keeping a small enough number of colours to be easily manipulated. Finally, a default classification based on predefined colour segmentation is first proposed and then iteratively refined by the user. The allocation of the colours to each class (vegetation elements versus background) is the most critical phase that needs to be interactive because colours depend both on illumination conditions and on canopy elements. At the end of this process a binary image, background versus vegetation elements (including both green and non-green elements) is obtained.

The CAN-EYE software computes biophysical variables from gap fraction as follows:

Effective LAI (LAI_{eff}): Among the several methods described in Weiss et al (2004), the effective LAI estimation in the CAN-EYE software is performed by model inversion. The effective LAI is estimated from the Plant Area Index (PAI) which is the variable estimated by CAN-EYE, as no distinction between leaves or other plant elements are made from the gap fraction estimates. PAI is very close to the effective LAI for croplands or shrublands when pictures are taken downward looking, whereas larger discrepancies are expected for forest when pictures are taken upward looking. Effective LAI is directly retrieved by inverting Eq. (1) (Poisson model) and assuming an ellipsoidal distribution of the leaf inclination using look-up-table (LUT) techniques.

$$P_0(\theta_v, \varphi_v) = e^{-N \cdot (\theta_v, \varphi_v)} = e^{-G \cdot (\theta_v, \varphi_v) \cdot \frac{LAI_{eff}}{\cos(\theta_v)}} \quad \text{Eq. (1)}$$

A large range of random combinations of LAI (between 0 and 10, step of 0.01) and ALA (Average Leaf Angle) (10° and 80°, step of 2°) values is used to build a database made of the corresponding gap fraction values (Eq.1) in the zenithal directions defined by the CAN-EYE user (60° for the DHP collection in this field campaign). The process consists then in selecting the LUT element in the database that is the closest to the measured P_0 . The distance (cost function C_k) of the k^{th} element of the LUT to the measured gap fraction is computed as the sum of two terms. The first term computes a weighted relative root mean square error between the measured gap fraction and the LUT one. The second term is the regularization term that imposes constraints to improve the PAI estimates. Two equations are proposed for the second “regularization” term:

(1) constraint used in CAN-EYE V5.1 on the retrieved ALA values that assume an average leaf angle close to 60° ± 03°, and

(2) constraint used in CAN-EYE V6.1 on the retrieved PAI value that must be close from the one retrieved from the zenithal ring at 57°. This constraint is more efficient, but it can be computed only when the 57° ring is available (i.e., $COI \geq 60^\circ$)

The software also proposed other ways of computing PAI and ALA effective using Miller’s formula (Miller, 1967) which assumed that gap fraction only depends from view zenith angle. Furthermore, the CAN-EYE makes an estimation using the Welles and Norman (1991) method used in LAI-2000 for 5 rings. These LAI2000-like estimates were not used here as are based on the same Miller’s formula but using limited angular sampling.

LAI: The actual LAI that can be measured only with a planimeter with however possible allometric relationships to reduce the sampling, is related to the effective leaf area index through:

$$LAI_{eff} = \lambda_0 \cdot LAI \quad \text{Eq. (2)}$$

where λ_0 is the clumping index. In CAN-EYE, the clumping index is computed using the Lang and Xiang (1986) logarithm gap fraction averaging method, although some uncertainties are associated to this method (Demarez et al., 2008). The principle is based on the assumption that vegetation elements are locally assumed randomly distributed. Values of clumping index given by CAN_EYE are in certain cases correlated with the size of the cells used to divide photographs. The values reported here were estimated with an average of the three results (CEV6.1, CEV5.1 and Miller).

As the CAN-EYE software provides different results (CEV6.1, CEV5.1 and Miller's) for LAI and LA_{eff} variables; an average LAI value was provided as ground estimate, and the standard deviation of the different method LAI estimates was reported as the uncertainty of the estimate (see associated 14_GM_25Mayo.xls file)

FCOVER is retrieved from gap fraction between 0 to 10°.

$$FCOVER = 1 - P_0 \cdot (0 - 10^\circ) \quad \text{Eq. (3)}$$

FAPAR: As there is little scattering by leaves in that particular spectral domain due to the strong absorbing features of the photosynthetic pigments, FAPAR is often assumed to be equal to FIPAR (Fraction of Intercepted Photosynthetically Active Radiation), and therefore to the gap fraction. The actual FAPAR is the sum of two terms, weighted by the diffuse fraction in the PAR domain: the 'black sky' FAPAR that corresponds to the direct component and the 'white sky' or the diffuse component.

The instantaneous "Black-sky FAPAR" ($FAPAR^{BS}$) is given at a solar position (date, hour and latitude). Depending on latitude, the CAN EYE software computes the solar zenith angle every solar hour during half the day (there is symmetry at 12:00). The instantaneous FAPAR is then approximated at each solar hour as the gap fraction in the corresponding solar zenith angle:

$$FAPAR^{BS}(\theta_S) = 1 - P_0 \cdot (\theta_S) \quad \text{Eq. (4)}$$

The daily integrated black sky or direct FAPAR is computed as the following:

$$FAPAR_{Day}^{BS} = \frac{\int_{sunset}^{sunrise} \cos(\theta_S) \cdot [1 - P_0 \cdot (\theta_S)] \cdot d\theta}{\int_{sunset}^{sunrise} \cos(\theta_S) \cdot d\theta} \quad \text{Eq. (5)}$$

4.2. SPATIAL SAMPLING SCHEME

A total of 43 ESUs (Elementary Sample Unit) of 6 different land cover types were characterized during the campaign (see Table 3). A pseudo-regular sampling was used

within each ESU of approximately 20x20 m². The centre of the ESU was geo-located using a GPS. The number of hemispherical photos per ESU ranges between 12 and 15.

Figure 9 shows the distribution of the sampling units over the experimental site. The ground measurements are spread across fields of corn, alfalfa and tree plantation (*Populus Alba*), as well as in shrublands. Ground dataset correspond to DHP images taken during the intensive field campaign.

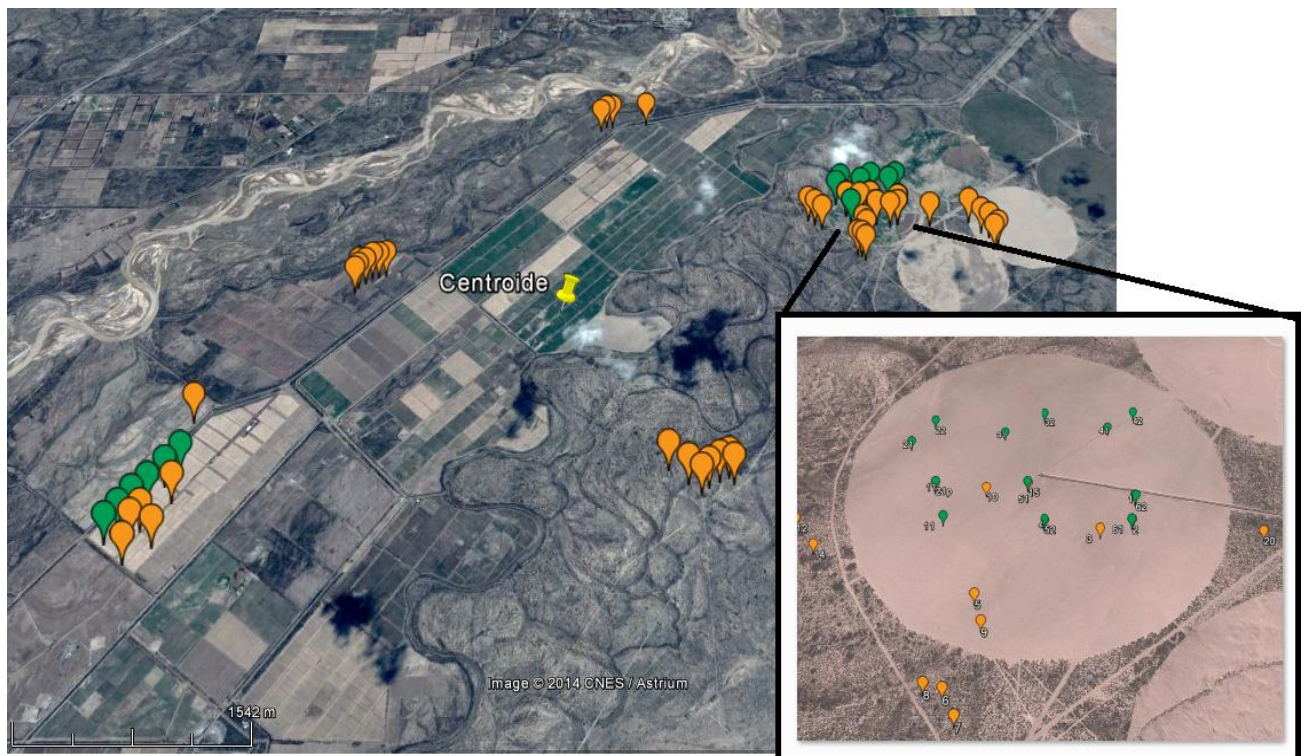


Figure 9: Distribution of the sampling units (ESU) over the study area. DHP sampling (in orange), PASTIS sampling (in green) over 25 de Mayo site, Argentina.

Table 3 summarizes the number of sampling units (ESUs) per each crop type acquired during the field campaigns.

Table 3: Summary of the field measurements in 25 de Mayo – La Pampa site.

ESU internal code	Number of ESU's
	First Campaign (9 th of February, 2014)
AL (Alfalfa)	9
SH (Shurbs)	14
G (Grasland)	5
C (Corn)	4
BS (Bare Soil)	1
TP (<i>Populus Alba</i>)	10
TOTAL	43

4.3. GROUND DATA

4.3.1. Data processing

The software CAN-EYE version V6.1 was used to process the DHP images. Figure 10 shows some examples of DHP over several ESUS.

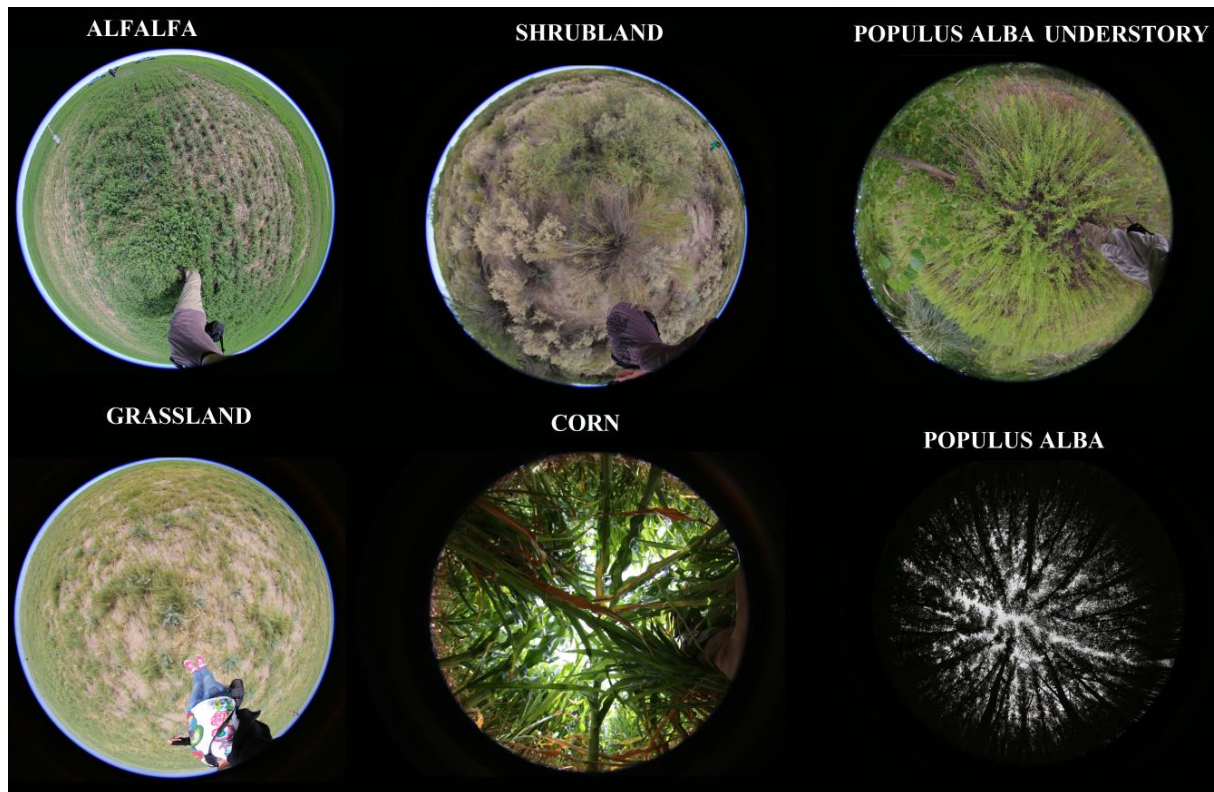


Figure 10: Digital Hemispherical Photographs acquired in 25 de Mayo, La Pampa, Argentina during the intensive campaign of 7-9 February 2014.

Figure 11 shows the results of the CAN-EYE processing carried out on shrubland area. Different results of the CAN-EYE processing are selected: the masking, the classification of vegetation and the image generated by the software. Other graphs are shown: the average gap fraction and the clumping factor versus view zenith angle.

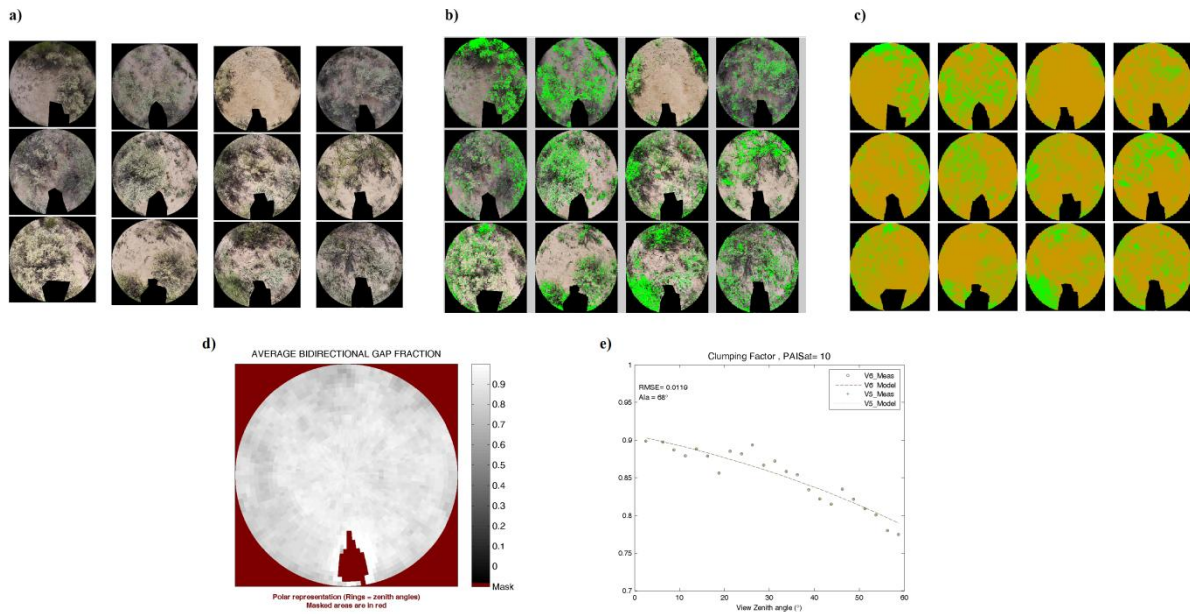


Figure 11: Results of the CAN-EYE processing carried out on shrubland area. (a) DHP images. (b, c) Classified images. (d) Average gap fraction and (e) the clumping factor versus view zenith angle.

- **ESUs with understory and overstory**

For several ESUs (26-28) with understory and overstory hemispherical images were acquired upward looking (overstory) and downward looking (understory) (Figure 12). The two sets of acquisitions were processed separately to derived LAI (effective and true), FCOVER and FAPAR. To compute FCOVER and FAPAR, the independency of the gaps inside the understory and the gaps inside the trees has been assumed. The ESU biophysical variable was then computed as:

- LAI (true, effective, LAI57) :

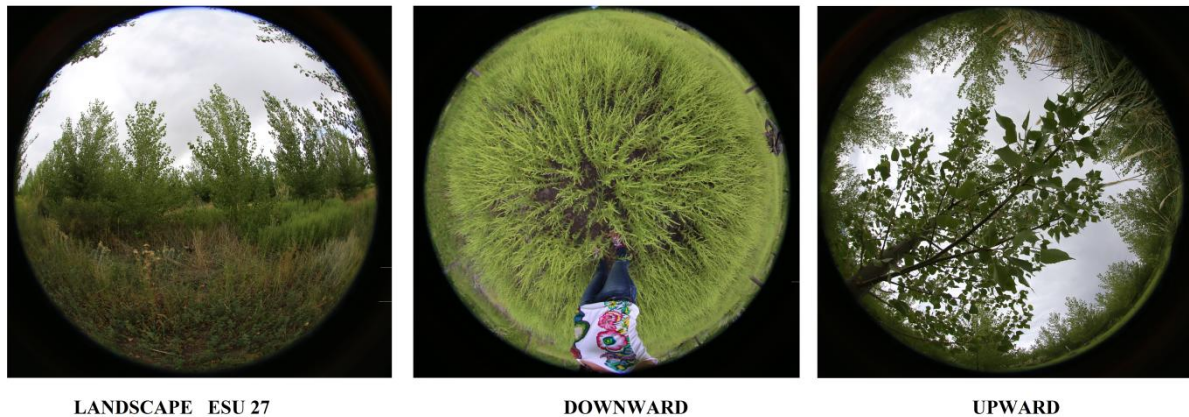
$$LAI = LAI_{ABOVE} + LAI_{BELOW}$$

- FCOVER: This way to get the total FCOVER/FAPAR is true for the local scales considered, a first order approximation.

$$FCOVER = 1 - (1 - FCOVER_{ABOVE}) \cdot (1 - FCOVER_{BELOW})$$

- FAPAR:

$$FAPAR = 1 - (1 - FAPAR_{ABOVE}) \cdot (1 - FAPAR_{BELOW})$$



LANDSCAPE ESU 27

DOWNWARD

UPWARD

Figure 12: DHP images for ESU 27, showing landscape (left), understory (middle), and overstory (right), 25 de Mayo Field Campaign in La Pampa – Argentina.

- **Heterogeneous ESUs showing non-stable CAN- EYE retrievals**

For some ESUs a quite large variation in the results of the CAN-EYE processing was detected, mainly in those ESUs where the surface appears to be heterogeneous (e.g. alfalfa) or the sky was cloudy. For instance, in the heterogeneous alfalfa cover, for the same ESU, some photos showed very dense vegetation, whereas others shots showed sparse vegetation (e.g. Figure 13). The processing with CAN-EYE was sensible to the picture selected for classification of green/soils elements. In order to reduce errors, we processed four times (two classifying vegetation elements and two classifying soil/sky elements) the more problematic ESUs. As a result, we compute the average value of the four processing and the standard deviation was provided as uncertainty. Note that the estimated LAI values are the average of the four processing with three methods (CE V6.1, CE V5.1, Miller's) each.



Figure 13: Several DHP images from ESU 1 (Alfalfa), 25 de Mayo Field Campaign in La Pampa – Argentina.

4.3.2. Content of the Ground Dataset

Each ESU is described according to a standard format. The header of the database is shown in Table 4.

Table 4: The Header used to describe ESUs with the ground measurements.

Column	Var.Name	Comment	
1	Plot #	Number of the field plot in the site	
2	Plot Label	Label of the plot in the site	
3	ESU #	Number of the Elementary Sampling Unit (ESU)	
4	ESU Label	Label of the ESU in the campaign	
5	Northing Coord.	Geographical coordinate: Latitude (°), WGS-84	
6	Easting Coord.	Geographical coordinate: Longitude (°), WGS-84	
7	Extent (m) of ESU (diameter)	Size of the ESU ⁽¹⁾	
8	Land Cover	Detailed land cover	
9	Start Date (dd/mm/yyyy)	Starting date of measurements	
10	End Date (dd/mm/yyyy)	Ending date of measurements	
11	Products*	Method	Instrument
12		Nb. Replications	Number of Replications
13		PRODUCT	Methodology
14		Uncertainty	Standard deviation

*LAI_{eff}, LAI, FAPAR and FCOVER

Figures 14 to 17 show the measurements obtained during the field experiment. Figure 14 shows the LAI_{eff}, with values ranging from 0.2 (Shrubs) to 4.2 (Tree Plantation, Corn). Similar distribution presents LAI, with higher values due to the clumping factor (Figure 15). Maximum values are up to 6 for Corn and slightly lower for Tree Plantation.

Figure 16 shows the FAPAR values covering the full dynamic range, with minimum values for shrublands (0.05-0.2), medium to high absorption values for alfalfa (around 0.6) and up to 0.9 for Tree Plantation. Slightly lower results were obtained for the FCOVER (Figure 17).

25 de Mayo site – 9th February, 2014

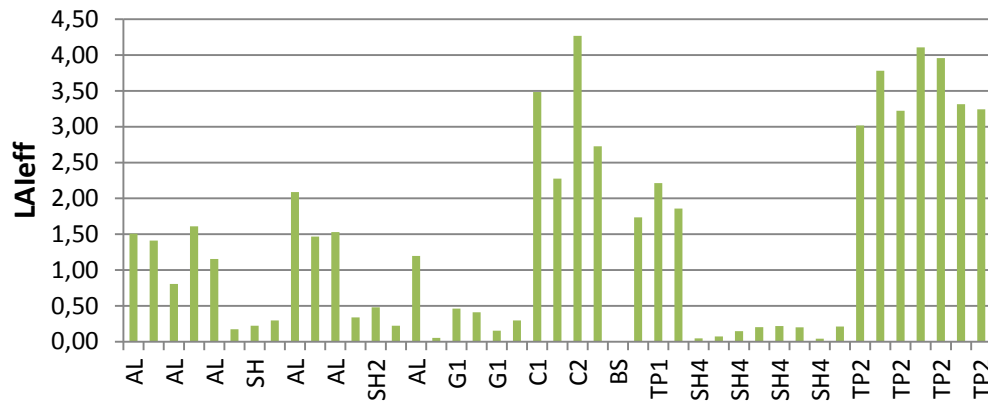


Figure 14: LAI_{eff} measurements acquired in 25 de Mayo site during the campaign of February 2014. Distribution by ESUS. (AL: Alfalfa, SH: Shrubland, G: Grassland, TP: Tree Plantation, BS: BareSoil)

25 de Mayo site – 9th February, 2014

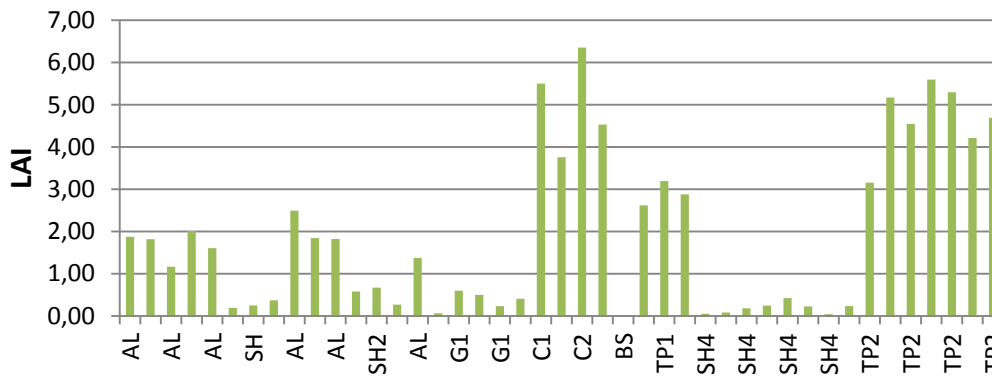


Figure 15: LAI measurements acquired in 25 de Mayo site during the campaign of 2014.

25 de Mayo site – 9th February, 2014

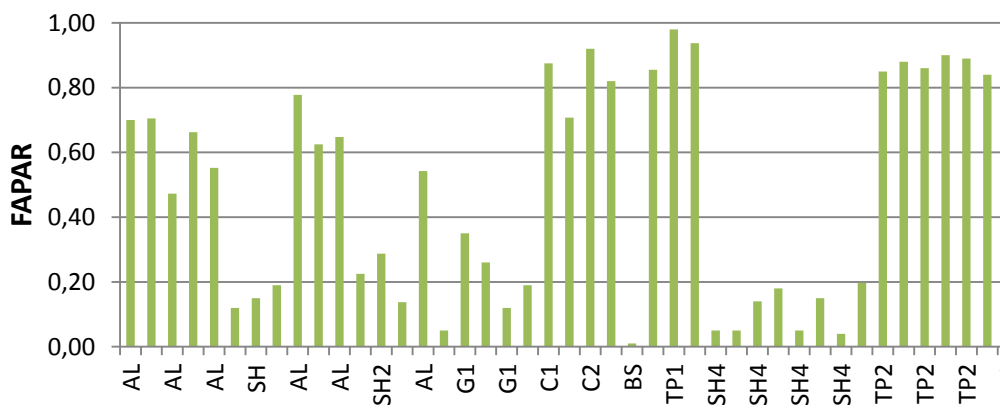


Figure 16: FAPAR measurements acquired in 25 de Mayo site during the campaign of 2014.

25 de Mayo site – 9th February, 2014

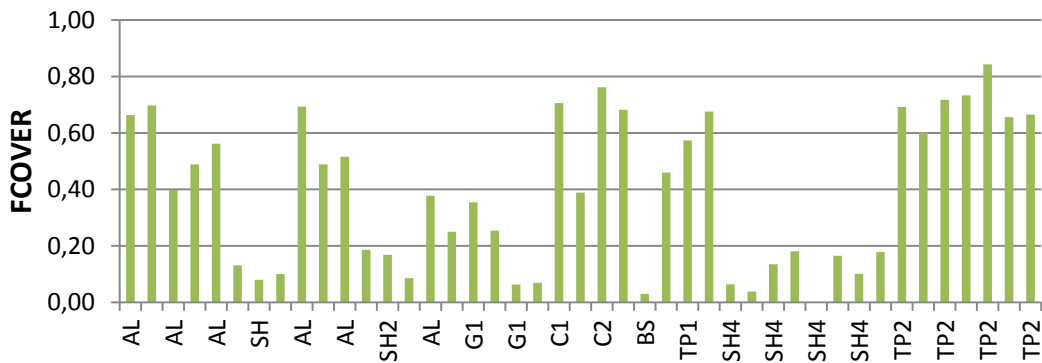


Figure 17: FCOVER measurements acquired in 25 de Mayo site during the campaign of 2014. . Distribution by ESUs. (AL: Alfalfa, SH: Shrubland, G: Grassland, TP: Tree Plantation, BS: BareSoil)

Figure 18 shows the distribution of the measured variables, covering the dynamic range of vegetation, with larger frequencies for lower values. For LA_{eff} and LAI, more frequent values are found at low values, while for FAPAR/FCOVER the distribution of values is higher for low or high values.

25 de Mayo site – 9th February, 2014

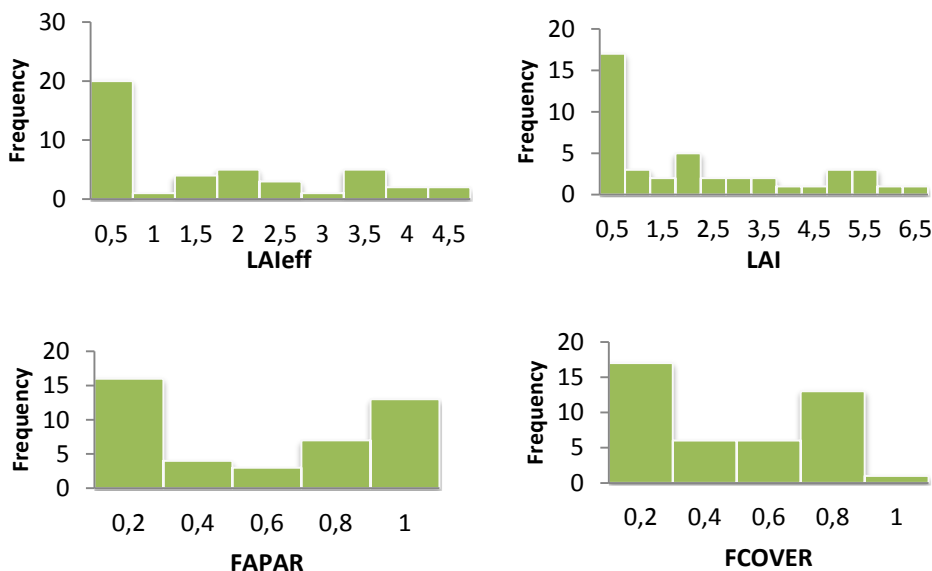


Figure 18: Distribution of the measured biophysical variables over the ESUs. 25 de Mayo site during the campaign of 9th February, 2014.

5. EVALUATION OF THE SAMPLING

5.1. PRINCIPLES

Based on previous field activities, the data set sampling was concentrated in the most representative areas. The number of ESUs was 43 for collected DHP data that were used for up-scaling.

5.2. EVALUATION BASED ON NDVI VALUES

The sampling strategy is evaluated using the SPOT5 image by comparing the NDVI distribution over the site with the NDVI distribution over the ESUs (Figure 19). As the number of pixels is drastically different for the ESU and whole site (WS) it is not statistically consistent to directly compare the two NDVI histograms. Therefore, the proposed technique consists in comparing the NDVI cumulative frequency of the two distributions by a Monte-Carlo procedure which aims at comparing the actual frequency to randomly shifted sampling patterns. It consists in:

1. computing the cumulative frequency of the N pixel NDVI that correspond to the exact ESU locations; then, applying a unique random translation to the sampling design (modulo the size of the image)
2. computing the cumulative frequency of NDVI on the randomly shifted sampling design
3. repeating steps 2 and 3, 199 times with 199 different random translation vectors.

This provides a total population of $N = 199 + 1$ (actual) cumulative frequency on which a statistical test at acceptance probability $1 - \alpha = 95\%$ is applied: for a given NDVI level, if the actual ESU density function is between two limits defined by the $N\alpha / 2 = 5$ highest and lowest values of the 200 cumulative frequencies, the hypothesis assuming that WS and ESU NDVI distributions are equivalent is accepted, otherwise it is rejected.

Figure 19 shows that the NDVI distribution of the 25 de Mayo - February, 2014 campaign is good over the whole site (comprised between the 5 highest and lowest cumulative frequencies). The sampling presents a bias towards higher NDVI values, as most of the area is covered by shrublands but our sampling was biased towards crops.

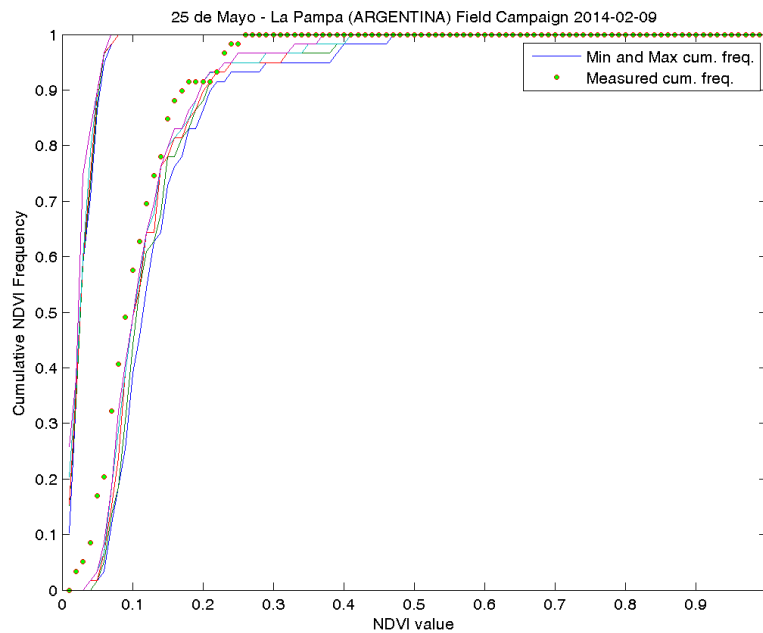


Figure 19: Comparison of NDVI (TOA) distribution between ESUs (green dots) and over the whole image (Blue line), 25 de Mayo – La Pampa site. Argentina (9th February 2014).

5.3. EVALUATION BASED ON CONVEX HULL: PRODUCT QUALITY FLAG.

The interpolation capabilities of the empirical transfer function used for up-scaling the ground data using decametric images is dependent of the sampling (Martinez et al., 2009). A test based on the convex hulls was also carried out to characterize the representativeness of ESUs and the reliability of the empirical transfer function using the different combinations of the selected bands (green, red, NIR and SWIR) of the SPOT5 image. A flag image is computed over the reflectances. The result on convex-hulls can be interpreted as:

- pixels inside the 'strict convex-hull': a convex-hull is computed using all the SPOT5 reflectances corresponding to the ESUs belonging to the class. These pixels are well represented by the ground sampling and therefore, when applying a transfer function the degree of confidence in the results will be quite high, since the transfer function will be used as an interpolator;
- pixels inside the 'large convex-hull': a convex-hull is computed using all the reflectance combinations ($\pm 5\%$ in relative value) corresponding to the ESUs. For these pixels, the degree of confidence in the obtained results will be quite good, since the transfer function is used as an extrapolator (but not far from interpolator);
- pixels outside the two convex-hulls: this means that for these pixels, the transfer function will behave as an extrapolator which makes the results less reliable. However,

having a priori information on the site may help to evaluate the extrapolation capacities of the transfer function.

Figure 20 shows the results of the Convex-Hull test (i.e., Quality Flag image) for the 25 de Mayo site over a 20x20 km² area around the central coordinate site. The strict and large convex-hulls are high around the test site (45 % over the 20x20 km² area and 75% over a 10x10 km² region around the centre). The QF map shows also that there is a quite important area where the transfer function behaves as extrapolator corresponding to shrublands areas far away from the croplands. Nevertheless, the results obtained in the maps seem to be reliable. Note that the Convex-Hull test provides information on the representativeness of the sampling, but not necessarily implies poor extrapolation capabilities of the transfer function.

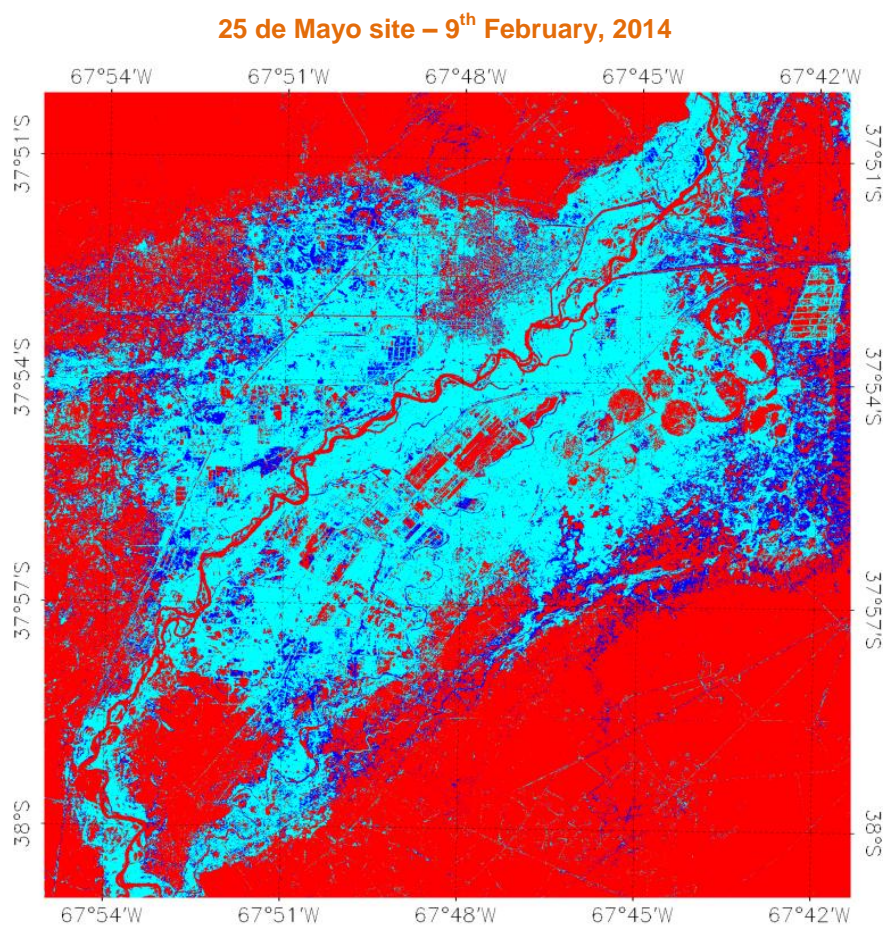


Figure 20: Convex Hull test over 20x20km² area centered at the test site: clear and dark blue correspond to the pixels belonging to the 'strict' and 'large' convex hulls. Red corresponds to the pixels for which the transfer function is extrapolating, 25 de Mayo- La Pampa (9th February 2014).

6. PRODUCTION OF GROUND-BASED MAPS

6.1. IMAGERY

The SPOT5 images were acquired the 9th February 2014 (see Table 5 for acquisition geometry). It corresponds to 4 spectral bands from 500 nm to 1750 nm with a nadir ground sampling distance of 10 m. For the transfer function analysis, the input satellite data used is Top of Atmosphere (TOA) reflectance. The original projection is UTM 19 South, WGS-84.

Table 5: Acquisition geometry of SPOT5 HRG 1 N1A data used for retrieving high resolution maps.

SPOT 5 METADATA	
Platform / Instrument	SP05 / HRG 1
Sensor	OPTICAL 10 m
Spectral Range	B1(green) : 0.5-0.59 μm B2(red) : 0.61-0.68 μm B3(NIR) : 0.78-0.89 μm B4(SWIR) : 1.58-1.75 μm
February 2014 campaign	
Acquisition date	2014-02-09 13:39:54
Incidence angle	-26.146228°
Viewing angle	-22.818947°
Illumination Azimuth angle	73.507466°
Illumination Elevation angle	43.210963°

6.2. THE TRANSFER FUNCTION

6.2.1. The regression method

If the number of ESUs is enough, multiple robust regression 'REG' between ESUs reflectance and the considered biophysical variable can be applied (Martínez et al., 2009): we used the 'robustfit' function from the Matlab statistics toolbox. It uses an iteratively re-weighted least squares algorithm, with the weights at each iteration computed by applying the bi-square function to the residuals from the previous iteration. This algorithm provides lower weight to ESUs that do not fit well.

The results are less sensitive to outliers in the data as compared with ordinary least squares regression. At the end of the processing, two errors are computed: weighted RMSE (using the weights attributed to each ESU) and cross-validation RMSE (leave-one-out method).

As the method has limited extrapolation capacities, a flag image (Figure 20), based on the convex hulls, is included in the final ground based map in order to inform the users on the reliability of the estimates.

6.2.2. Band combination

Figure 21 shows the results obtained for all the possible band combinations using TOA reflectance. Attending specifications of minimal noise and maximal sensitivity it has been chosen for the intensive campaign (7th - 9th February): band 1 (green), band 2 (red) band 3 (Near Infrared) and band 4 (Short Wave Infrared) combination of (1,2,3,4) = (G, R, N, S).

These combinations on reflectance were selected since they provide a good compromise between the cross-validation RMSE, the weighted RMSE (lowest value) and the number of rejected points.

6.2.3. The selected Transfer Function

The applied transfer function is detailed in Table 6, along with its weighted and cross validated errors.

Table 6: Transfer function applied to the whole site for LA_{leff}, LAI, FAPAR and FCOVER. RW for weighted RMSE, and RC for cross-validation RMSE.

Variable	Band Combination	RW	RC
First Campaign			
LA_{leff}	$0.735 - 0.029 \cdot (\text{SWIR}) - 0.044 \cdot (\text{NIR}) + 0.043 \cdot (\text{R}) + 0.025 \cdot (\text{G})$	0.703	0.910
LAI	$0.939 - 0.044 \cdot (\text{SWIR}) - 0.062 \cdot (\text{NIR}) + 0.061 \cdot (\text{R}) + 0.036 \cdot (\text{G})$	0.98	1.201
FAPAR	$-0.043 - 0.006 \cdot (\text{SWIR}) - 0.014 \cdot (\text{NIR}) + 0.012 \cdot (\text{R}) + 0.008 \cdot (\text{G})$	0.149	0.226
FCOVER	$-0.064 - 0.003 \cdot (\text{SWIR}) - 0.014 \cdot (\text{NIR}) + 0.012 \cdot (\text{R}) + 0.006 \cdot (\text{G})$	0.175	0.189

25 de Mayo site – 9th February, 2014

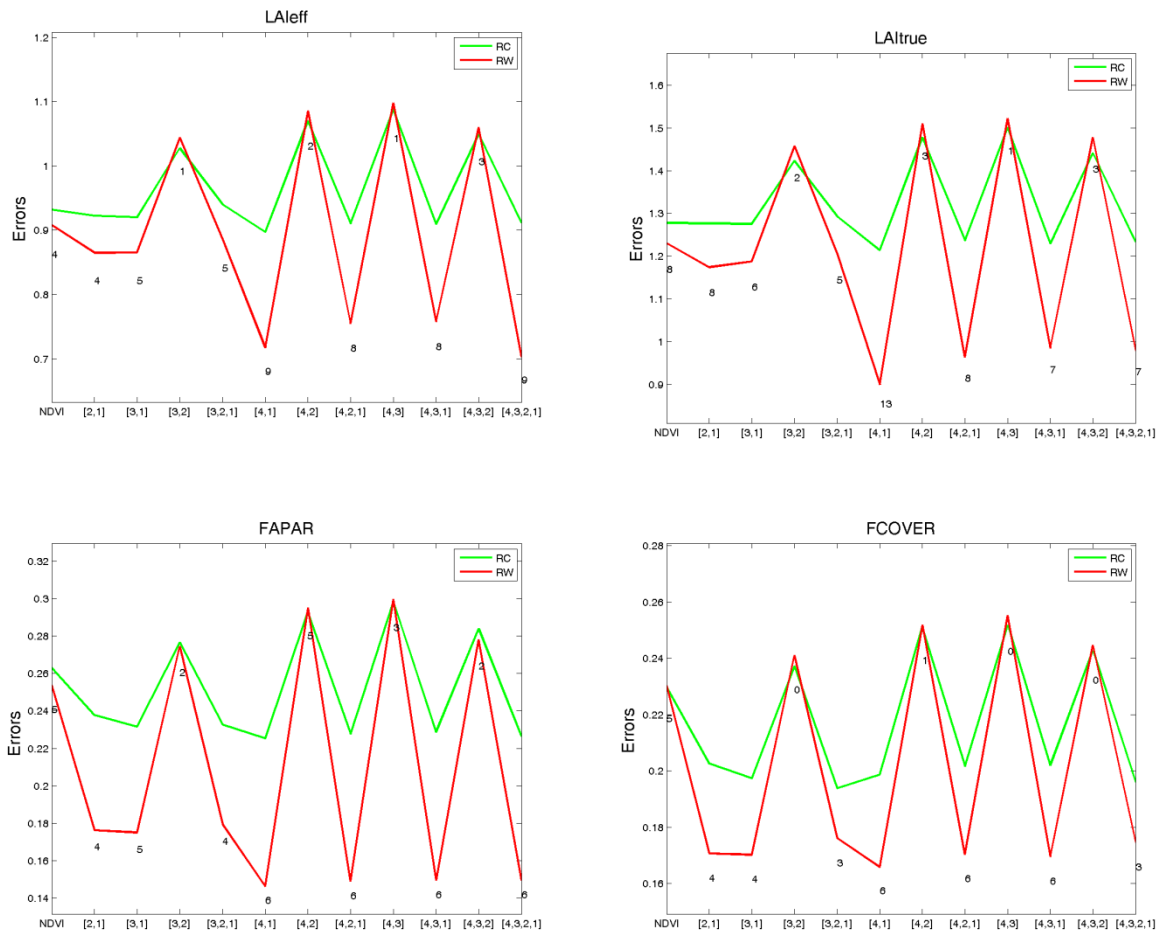


Figure 21: Test of multiple regression (TF) applied on different band combinations. Band combinations are given in abscissa (2=G, 3=RED, 4=NIR and 5=SWIR). The weighted root mean square error (RMSE) is presented in red along with the cross-validation RMSE in green. The numbers indicate the number of data used for the robust regression with a weight lower than 0.7 that could be considered as outliers.

25 de Mayo site – 9th February, 2014

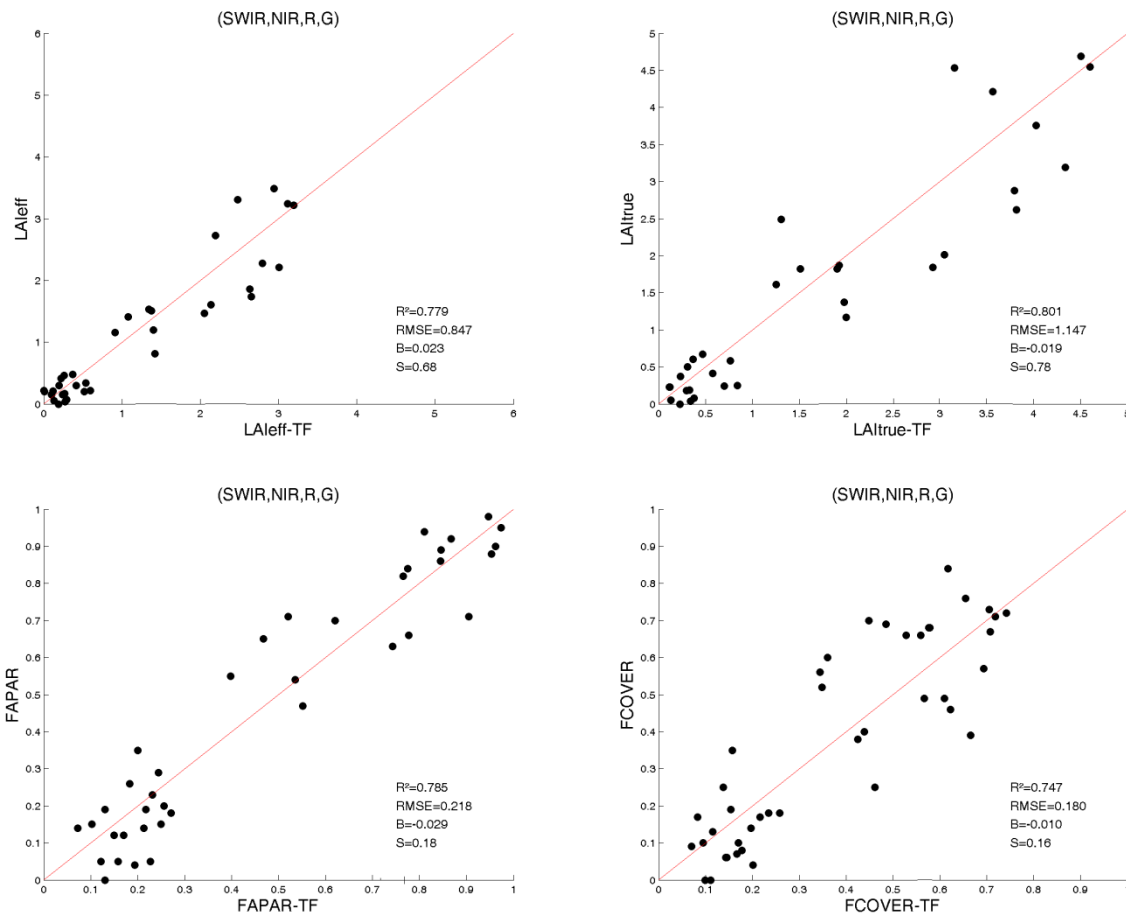


Figure 22: LAleff, LAI, FAPAR and FCOVER results for regression on reflectance using 4 bands combination.

Figure 22 shows scatter-plots between ground observations and their corresponding transfer function (TF) estimates for the selected bands combinations. A good correlation is observed for the LAleff, LAI, FAPAR and FCOVER with points distributed along the 1:1 line, and no bias, but showing some scattering. The different architecture of the several vegetation types (from grasslands to high trees) could contribute to the observed scattering in an empirical relationship.

6.3. THE HIGH RESOLUTION GROUND BASED MAPS

The high resolution maps are obtained applying the selected transfer function (Table 6) to the SPOT5 TOA reflectance. Figures 23 and 24 present the TF biophysical variables over a 20x20 km² area. Figure 20 shows the Quality Flag included in the final product.

25 de Mayo site – 9th February, 2014

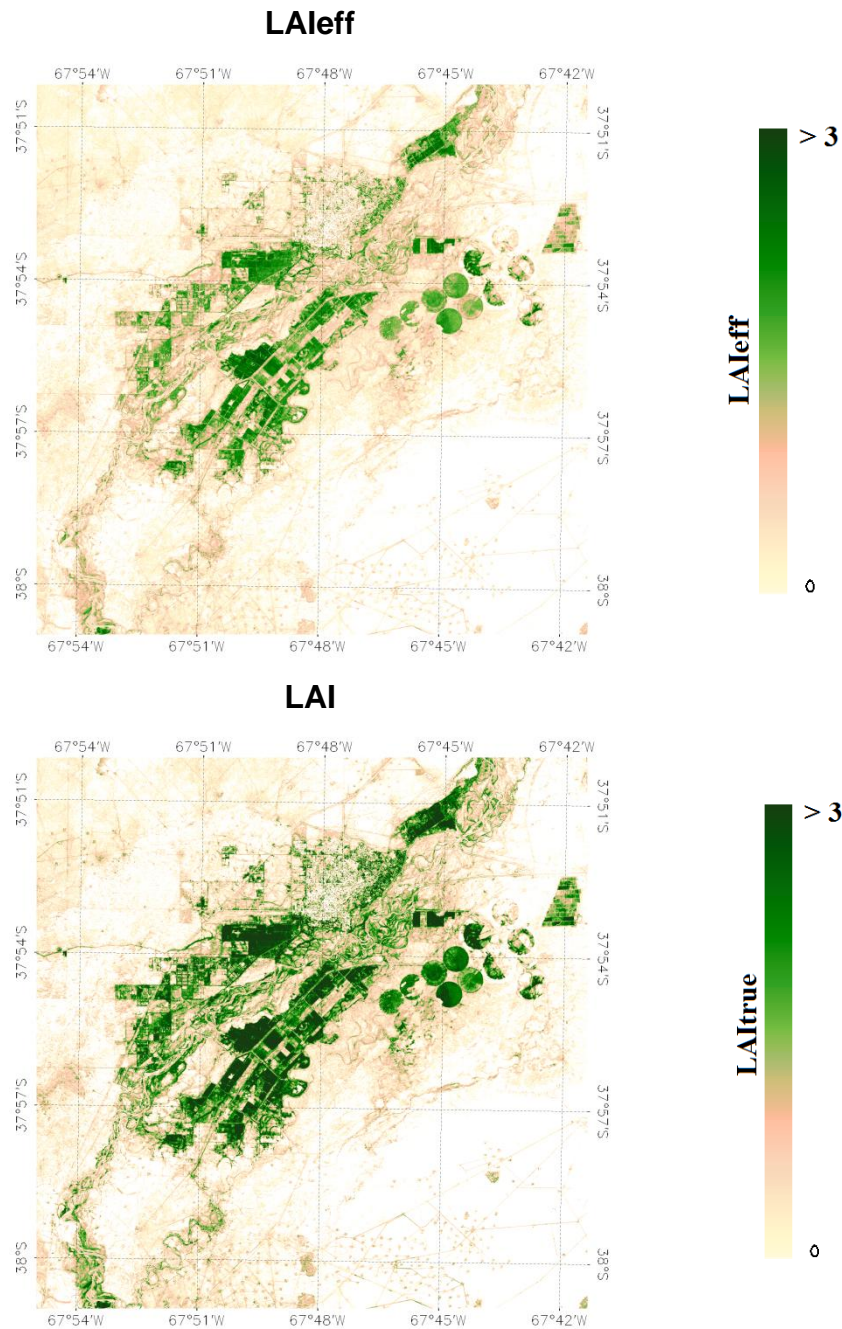


Figure 23: Ground-based LAI maps (20x20 km²) retrieved on the 25 de Mayo- La Pampa site (Argentina). Top: LAI_{eff}. Bottom: LAI. (9th February 2014).

25 de Mayo site – 9th February, 2014

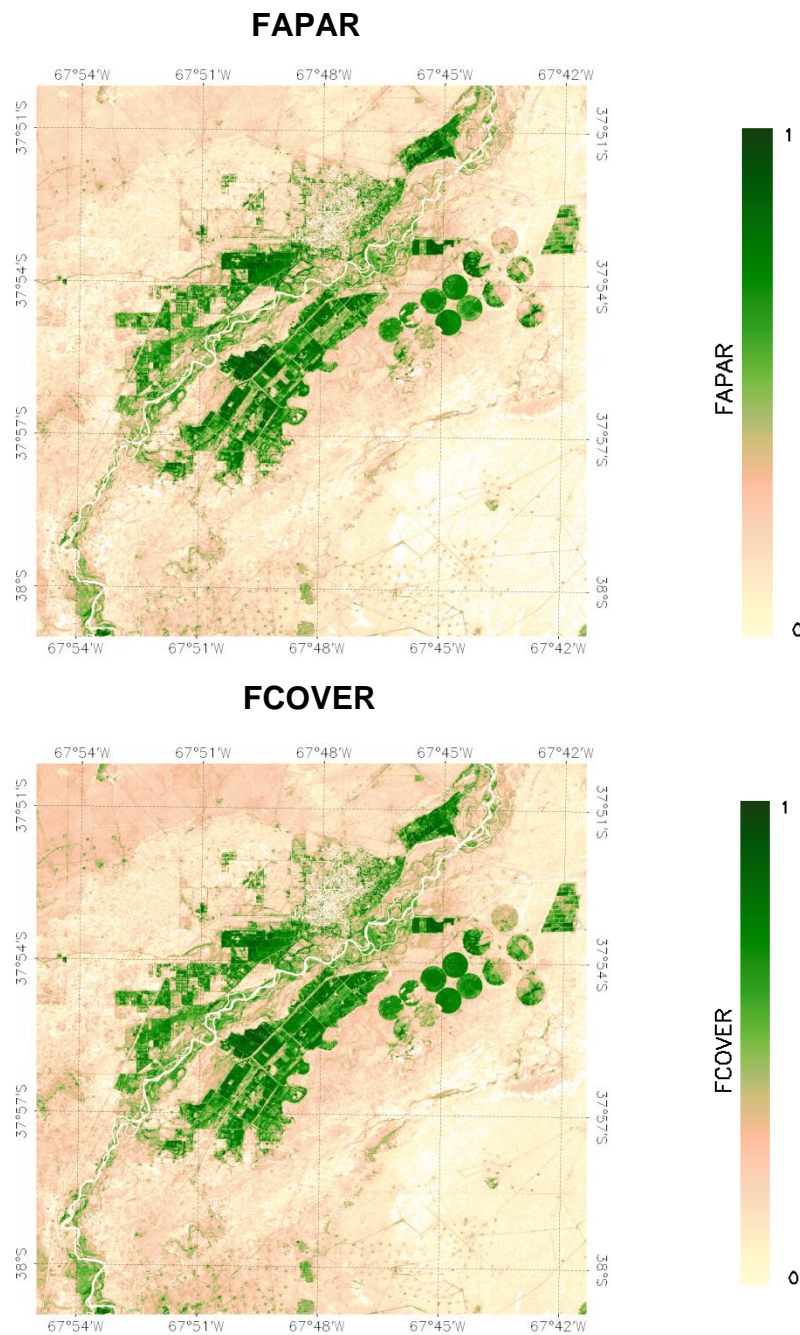


Figure 24: Ground based FAPAR and FCOVER maps (20x20 km²) retrieved on the 25 de Mayo - La Pampa site (Argentina). Top: FAPAR. Bottom: FCOVER. (9th February 2014).

6.3.1. Selected zones for validation

Several zones for validation of PROBA-V satellite products at 1 km and 333 m spatial resolution were selected (Figure 25) over several 1x1 km² (Table 8) and 3x3 km² (Table 7) areas showing variability in land cover types (i.e., croplands, shrublands, tree plantation) and large confidence of the transfer function as ground data was collected inside these areas. Both tables summarize the mean and standard deviation values and the centre coordinates for these areas.

Table 7. Mean values and standard deviation (STD) of the HR biophysical maps for the selected 3 x 3 km² areas at 25 de Mayo site.

NAME	COORDINATES		LAI _{eff}		LAI		FAPAR		FCOVER	
	LATITUDE	LONGITUDE	MEAN	STD	MEAN	STD	MEAN	STD	MEAN	STD
Alfalfa	-37.907	-67.746	0.93	0.74	1.30	1.08	0.39	0.24	0.32	0.19
Shrub	-37.939	-67.789	0.31	0.41	0.42	0.59	0.19	0.13	0.16	0.10

Table 8. Mean values and standard deviation (STD) of the HR biophysical maps for the selected 1x1 km² areas at 25 de Mayo site.

NAME	COORDINATES		LAI _{eff}		LAI		FAPAR		FCOVER	
	LATITUDE	LONGITUDE	MEAN	STD	MEAN	STD	MEAN	STD	MEAN	STD
Shrub	-37.939	-67.789	0.20	0.20	0.25	0.29	0.17	0.07	0.15	0.05
Corn	-37.940	-67.833	1.71	0.82	2.43	1.19	0.62	0.22	0.48	0.15
Tree plantation	-37.928	-67.833	2.27	0.78	3.25	1.14	0.75	0.23	0.55	0.17
Alfalfa	-37.915	-67.771	1.23	0.59	1.74	0.86	0.50	0.19	0.40	0.15

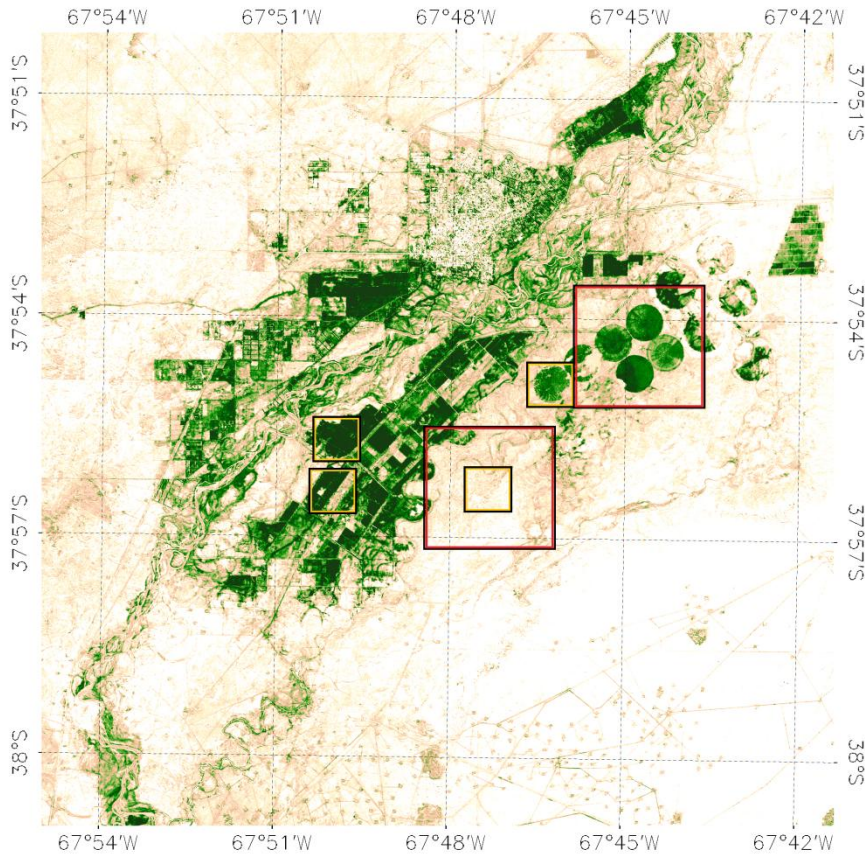


Figure 25: Selected areas for validation at the 3x3 km² (in red) and 1x1 km² (in yellow). Background HR LAI map (20x20 km²), 25 de Mayo site, Argentina (9th February 2014).

Table 9 describes the content of the geo-biophysical maps in the “BIO_YYYYMMDD_SPOT5_25MAYO_ETF_20x20” files.

Table 9: Content of the dataset.

Parameter	Dataset name	Range	Variable Type	Scale Factor	No Value
LAI effective	LAIeff	[0, 7]	Integer	1000	-1
LAI	LAI	[0, 7]	Integer	1000	-1
FAPAR	FAPAR	[0, 1]	Integer	10000	-1
Fraction of Vegetation Cover	FCOVER	[0, 1]	Integer	10000	-1
Quality Flag	QFlag	0,1,2 (*)	Integer	N/A	-1

(*) 0 means extrapolated value (low confidence), 1 strict interpolator (best confidence), 2 large interpolator (medium confidence)

7. CONCLUSIONS

The FP7 ImagineS project continues the innovation and development activities to support the operations of the Copernicus Global Land service. One of the ImagineS demonstration sites is located at the "Río Colorado" basin, close to the "25 de Mayo" village, in La Pampa (Argentina), over irrigated crops in the semiarid environment of La Pampa.

This report first presents the ground data collected during an intensive field campaign on 7th - 9th of February of 2014. The dataset includes 43 elementary sampling units where digital hemispherical photographs were taken and processed with the CAN-EYE software to provide LAI, LAI_{eff}, FAPAR and FCOVER values to characterize the natural vegetation of the area (shrublands) as well as several croplands and tree plantation plots in the study area.

Secondly, high resolution ground-based maps of the biophysical variables have been produced over the site. Ground-based maps have been derived using high resolution imagery (SPOT-5) according with the CEOS LPV recommendations for validation of low resolution satellite sensors. Transfer functions have been derived by multiple robust regressions between ESUs reflectance and the several biophysical variables. The spectral bands combination to minimize errors (weighted RMSE and cross-validation RMSE) were band 1 (green), band 2 (red) band 3 (Near Infrared) and band 4 (Short Wave Infrared) combination. The RMSE values for the several transfer function estimates are 0.85 for LAI_{eff}, 1.15 for LAI, 0.22 for FAPAR and finally 0.18 for FCOVER, with no bias but some scattering.

The quality flag map based on the convex-hull analysis shows very good quality around the centre of the image (75 % at 10x10 km² around the Centrum), with a large area in the contours of the image corresponding to shrublands areas far away from the sampled area, where the transfer function behaves as extrapolator, however the results obtained in the maps seem to be reliable although with less confidence.

The biophysical variable maps are available in geographic (UTM 19 South projection WGS-84) coordinates at 10 m resolution. Mean values and standard deviation for LAI_{eff}, LAI, FCOVER and FAPAR was computed over several areas of 3x3 km² and 1x1 km².

8. ACKNOWLEDGEMENTS

This work is supported by the FP7 IMAGINES project under Grant Agreement N°311766. SPOT 5-HR imagery are provided through the GMES Services Coordinated Interface (SCI) ESA service. This work is done in collaboration with the consortium implementing the Global Component of the Copernicus Land Service.

Thanks to the *INTA – 25 de Mayo* for the support and the organization of the Field Campaign, and the facilities which allow us to characterize the site.

9. REFERENCES

- Baret, F and Fernandes, R. (2012). Validation Concept. VALSE2-PR-014-INRA, 42 pp.
- Camacho, F., Cernicharo, J., Lacaze, R., Baret, F., and Weiss, M. (2013). GEOV1: LAI, FAPAR Essential Climate Variables and FCOVER global time series capitalizing over existing products. Part 2: Validation and intercomparison with reference products. *Remote Sensing of Environment*, 137: 310-329.
- Cabrera, A.L. (1976). Regiones Fitogeográficas Argentinas. En : W.F. Kugler (Ed.). Enciclopedia Argentina de Agricultura y Jardinería. Editorial ACME. Buenos Aires. Tomo 2 Fascículo 1.85 pp.
- Demarez, V., Duthoit, S., Baret, F., Weiss, M. and Dedieu, G. (2008). Estimation of leaf area and clumping indexes of crops with hemispherical photographs. *Agricultural and Forest Meteorology*. 148, 644-655.
- Fernandes, R., Plummer, S., Nightingale, J., et al. (2014). Global Leaf Area Index Product Validation Good Practices. CEOS Working Group on Calibration and Validation - Land Product Validation Sub-Group. *Version 2.0: Public version made available on LPV website*.
- Martínez, B., García-Haro, F. J., & Camacho, F. (2009). Derivation of high-resolution leaf area index maps in support of validation activities: Application to the cropland Barrax site. *Agricultural and Forest Meteorology*, 149, 130–145.
- Miller, J.B. (1967). A formula for average foliage density. *Aust. J. Bot.*, 15:141-144
- Morici, E. ; Muiño, W ; Ernst, R ; Poey, S. (2006). Efecto de la distancia a la aguada sobre la estructura del estrato herbáceo en matorrales de Larrea sp. Pastoreados por bovinos en zonas áridas de Argentina. *Archivos de Zootecnia*. Vol. 55. Nº 210. Universidad de Córdoba España. 149-159 p.
- Morisette, J. T., Baret, F., Privette, J. L., Myneni, R. B., Nickeson, J. E., Garrigues, S., et al. (2006). Validation of global moderate-resolution LAI products: A framework proposed within the CEOS land product validation subgroup. *IEEE Transactions on Geoscience and Remote Sensing*, 44, 1804–1817.
- Weiss, M., Baret, F., Smith, G.J., Jonckheere, I. and Coppin, P., (2004). Review of methods for in situ leaf area index (LAI) determination. Part II. Estimation of LAI, errors and sampling. *Agricultural and Forest Meteorology*. 121, 37–53.
- Weiss M. and Baret F. (2010). CAN-EYE V6.1 User Manual
- Welles, J.M. and Norman, J.M., 1991. Instrument for indirect measurement of canopy architecture. *Agronomy J.*, 83(5): 818-825.